





Observation of site-controlled localized charged excitons in CrI₃/WSe₂ heterostructures

Arunabh Mukherjee¹, Kamran Shayan ¹, Lizhong Li^{2,3}, Jie Shan ^{2,3,4}, Kin Fai Mak ^{2,3,4} & A. Nick Vamivakas ^{1,5,6,7}✉

Isolated spins are the focus of intense scientific exploration due to their potential role as qubits for quantum information science. Optical access to single spins, demonstrated in III-V semiconducting quantum dots, has fueled research aimed at realizing quantum networks. More recently, quantum emitters in atomically thin materials such as tungsten diselenide have been demonstrated to host optically addressable single spins by means of electrostatic doping the localized excitons. Electrostatic doping is not the only route to charging localized quantum emitters and another path forward is through band structure engineering using van der Waals heterojunctions. Critical to this second approach is to interface tungsten diselenide with other van der Waals materials with relative band-alignments conducive to the phenomenon of charge transfer. In this work we show that the Type-II band-alignment between tungsten diselenide and chromium triiodide can be exploited to excite localized charged excitons in tungsten diselenide. Leveraging spin-dependent charge transfer in the device, we demonstrate spin selectivity in the preparation of the spin-valley state of localized single holes. Combined with the use of strain-inducing nanopillars to coordinate the spatial location of tungsten diselenide quantum emitters, we uncover the possibility of realizing large-scale deterministic arrays of optically addressable spin-valley holes in a solid state platform.

¹The Institute of Optics, University of Rochester, Rochester, NY, USA. ²School of Applied and Engineering Physics, Cornell University, Ithaca, NY, USA. ³Kavli Institute at Cornell for Nanoscale Science, Ithaca, NY, USA. ⁴Laboratory of Atomic and Solid State Physics, Cornell University, Ithaca, NY, USA. ⁵Materials Science, University of Rochester, Rochester, NY, USA. ⁶Department of Physics and Astronomy, University of Rochester, Rochester, NY, USA. ⁷Center for Coherence and Quantum Optics, University of Rochester, Rochester, NY, USA. ✉email: nick.vamivakas@rochester.edu

Photonic integrated circuits are advancing the state-of-the-art in quantum and classical information processing due to desirable properties like high operating speeds and low energy consumption¹. In this context, atomically thin semiconducting transition metal dichalcogenides (TMDs) have emerged as a unique platform that offers a material interface to photon polarization via the coupled spin–valley degree of freedom of its charge carriers^{2–5}. Consequently, TMD-based optically driven valleytronic devices⁶ have gained interest as potential candidates for beyond complementary metal-oxide-semiconductor (CMOS) technology. These devices operate by coupling the different circular polarizations of light with degenerate inequivalent local energy extrema (referred to as valleys^{3–5}) in the electronic band structure—valley specific addressing is accomplished via the handedness of light polarization^{3–8}.

Due to reduced dielectric screening in the two-dimensional (2D) plane, excitonic species strongly dominate the optical response of atomically thin TMDs^{9,10}. 2D excitons, like the neutral (X^0) and charged excitons (X^\pm , also known as trions), have been shown to inherit the valley character from the single-particle electronic band structure^{3–8,11}. Interestingly, the valley physics holds even for the case of localized neutral excitons^{12–15} and trions^{16–18}, provided the confinement length scale is larger than the Bohr radius of the excitons (~1 nm). A localized positive trion, for example, can be described as a bound state of three charges, an electron and a hole in one valley and another hole in the opposite valley. Such a localized trion radiatively relaxes to a ground state of one spin–valley hole—the detection of a circularly polarized photon is a projective measurement of the hole into one of the two possible spin–valley states. It is predicted that this hole will preserve its spin orientation for at least a few ns¹⁷ which may be sufficient for performing several quantum gate operations, provided that appropriate steps like pulsed optical excitation and post-selection to disregard trion re-trapping events are performed.

Although generating quantum confined trions in tungsten diselenide (WSe_2) has been previously realized by electrostatic doping^{16–18} in a van der Waals heterostructure (HS), the lack of ability to position the quantum emitter and the use of significant bias voltage for electrostatic doping limits the scalability and economical fabrication of optically driven valleytronic devices. Furthermore, electrostatic doping is not spin-selective, thus preventing any spin selectivity of the trions unless polarization selection schemes in the excitation and collection optics are used. Thus, spin-oriented quantum confined trions, excited by means of band-structure engineering, provides a pathway to circumvent the previous. Recently, it has been shown that 2D positive trions in a type-II HS can be formed by coupling chromium triiodide (CrI_3) thin films to a monolayer WSe_2 ¹⁹. Spin-polarized charge transfer between CrI_3 and WSe_2 results in a finite intensity contrast between the opposite circularly polarized positive trions even at no applied magnetic fields. The previous points to the possibility of forming site-controlled localized charged excitons with spin selectivity in WSe_2/CrI_3 if placed onto patterned nanopillar arrays^{20,21}.

In this work, we use band-structure engineering to create localized X^+ in monolayer WSe_2 which is interfaced with bilayer CrI_3 . The type-II band alignment between the two materials promotes p-doping of WSe_2 via charge transfer. We first show the existence of charge transfer using photoluminescence (PL) from the 2D positive trion. At locations of strain-inducing nanopillars, we observe quantum emitters, positive trions, that do not exhibit fine-structure splitting (FSS) due to quenched electron–hole exchange interactions—this is the hallmark of 0D trions¹⁷. We confirm the trionic character by using polarization-resolved magneto-PL experiments. We also demonstrate finite spin

selectivity in the 0D X^+ at no applied magnetic fields due to the spin-dependent charge transfer in the HS. Our work thus demonstrates site-controlled localized trions with spin selectivity in atomically thin materials.

Results

Optical response of the device on and off nanopillars. A schematic of our van der Waal HS device is shown in Fig. 1a. An optical micrograph of the device is shown in Supplementary Fig. 1. The HS is placed on a nanopillar array inducing strain on the HS at specific locations. The nanopillar array promotes localization of single excitons which is of central importance in this work. A bilayer CrI_3 is exfoliated and layered with monolayer WSe_2 in an N_2 environment and encapsulated with hBN (see “Methods”). A consequence of the type-II band alignment between WSe_2 and CrI_3 is charge-hopping of charge carriers that results in hole doping of WSe_2 ¹⁹. Figure 1b demonstrates how the type-II band alignment between WSe_2 and CrI_3 can promote hole doping of WSe_2 . This is manifested in the dominance of positively charged excitonic species PL. We show typical PL spectra on and off nanopillars in Fig. 1c, d in the HS region. The broad spectrum shown in Fig. 1c is consistent with previous observations^{19,22} and can be attributed to delocalized X^+ species. In contrast to this broad spectrum, in the vicinity of the nanopillars, we observe multiple narrow linewidth emission lines. The strain gradients induced by the nanopillars lead to such sharp emission lines with linewidths of 200–500 μ eV. Some of the emission lines occur in pairs (doublets) while there also are emissions with only one peak (singlets) at no applied magnetic field. The doublets are due to localized neutral excitons (0D X^0). The FSS occurs due to anisotropic electron and hole exchange interactions in an asymmetric confinement potential. In contrast, the positively charged 0D X^+ in WSe_2 exhibits a singlet hole-spin configuration that quenches the electron–hole exchange interactions. A tell-tale signature of localized charged excitons is the absence of FSS at zero magnetic field¹⁷.

To explain the origin of the charge-hopping between WSe_2 and CrI_3 , we consider the spatial band-diagram in Fig. 1b. The WSe_2 band structure consists of valleys at the six corners of the first Brillouin Zone. The valleys located at the opposite edges (labeled as K and K') can be accessed using opposite circularly polarized photons (σ_\pm). This phenomenon, known as spin–valley locking, stems from spin–orbit interactions that renders both the conduction and valence bands of each valley spin-polarized. The red and green levels shown are spin up and down, respectively. We also show the conduction and valence band levels of CrI_3 . The lowest unoccupied conduction band consists of e_g levels^{23,24} pointing in the direction of the applied magnetic field¹⁹. As a result these empty spin-polarized states e_g orbitals (shown in blue) can accept the spin-polarized electrons from one of the K or K' valleys. For the K' valley of WSe_2 , electrons prefer to move to CrI_3 whereas the holes move in the opposite way, thereby p-doping WSe_2 . Consequently, at high excitation powers, the PL spectrum is dominated by delocalized positively charged exciton species X^+ which is composed of two holes located in opposite valleys and one electron in one of those valleys. Furthermore, this type of charge distribution is valley sensitive and is weaker for the K valley in WSe_2 when the applied magnetic field pointing in the +z direction. This leads to brighter PL from X^+ involving the electrons located in the K valley. The photo-emission process in the energy–momentum space is depicted in Fig. 1c(i). The recombination of the e–h pair releases a circularly polarized photon and the extra hole is left behind the K' valley. The PL spectrum of the delocalized X^+ from a region between two nanopillars in the HS is shown in Fig. 1c(ii).

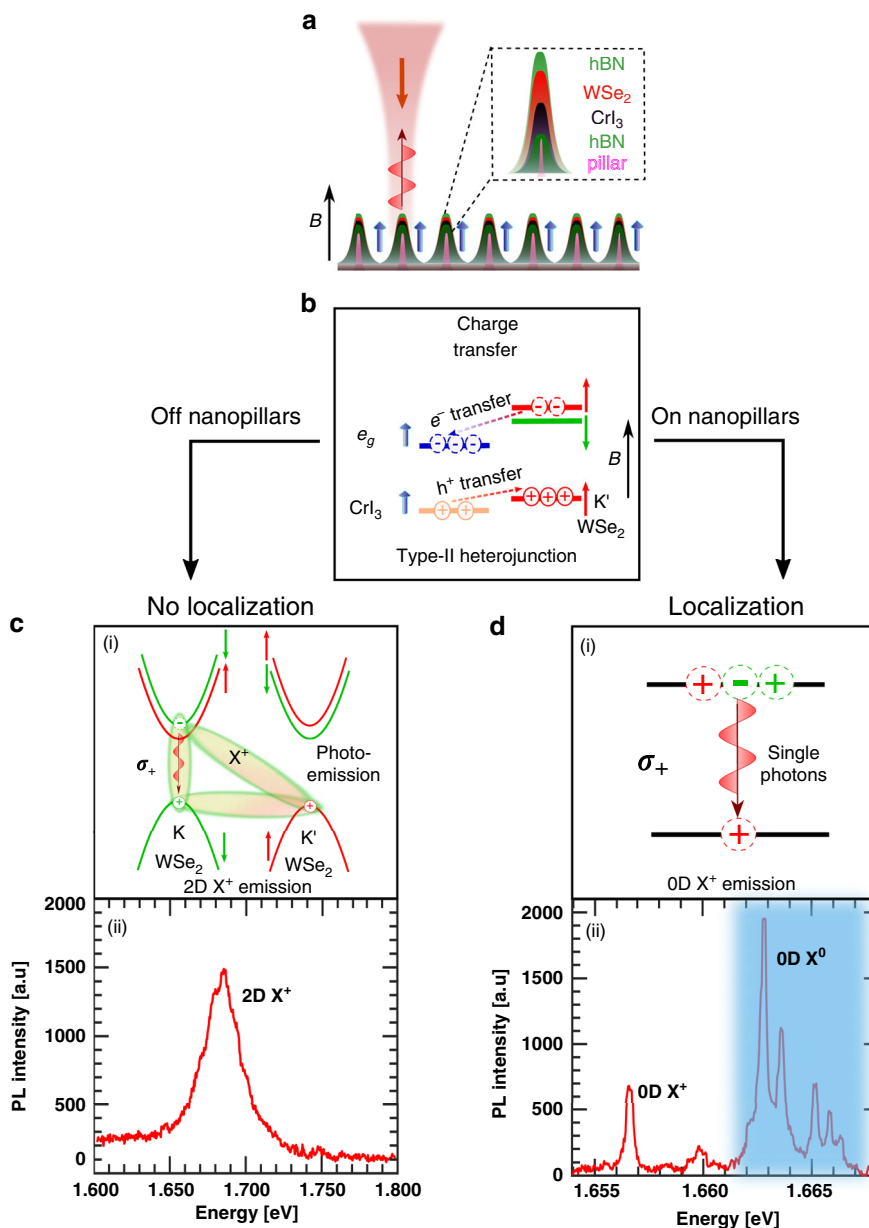


Fig. 1 **CrI₃/WSe₂ heterostructure stamped onto nanopillar arrays.** **a** A schematic illustration of the device structure showing the ordering of the atomically thin layers in the device. Boxed inset zooms into the region of one nanopillar. **b** Charge-hopping due to Type-II heterojunction results in highly p-doped WSe₂. Spins of the conduction and valence bands of WSe₂ (CrI₃) are shown with red and green (blue) arrows. **c** Photo-emission process of 2D X⁺ with an extra hole in the K' valley (top); A typical PL spectrum of the heterostructure off the nanopillars showing the prominence of the 2D X⁺ emission due to hole doping at no applied magnetic field (bottom). **d** Localization emission process for a OD X⁺ leading to a single hole in the K' valley (top); PL spectrum at zero magnetic field on the nanopillars showing multiple OD X⁺ and OD X⁰ emission lines (bottom).

We now employ the charge-hopping phenomenon to explain the observation of charged single localized excitons. It has been shown that strain, induced by means of nanopillars^{20,21}, or randomly occurring nano-bubbles²⁵, facilitate the localization of neutral excitons (OD X⁰). Upon significant p-doping, the OD X⁰ undergo a hole-capture process to result in OD X⁺. Unlike previous reports^{17,18}, our device architecture circumvents the need for electrical gating. The excited state of OD X⁺, akin to the delocalized 2D X⁺, consists of two holes and a single electron which upon radiative relaxation leaves behind a single localized hole. The spin of this hole is determined by the circular polarization of the emitted photon. The process for a spin-up extra hole has been shown in Fig. 1d

(i) and an exemplary PL spectra on a nanopillar site shown in Fig. 1d(ii).

Spin-dependent charge transfer in the CrI₃/WSe₂ HS. To experimentally prove the existence of spin-dependent charge transfer between CrI₃ and WSe₂, we performed circular polarization-resolved magneto-PL measurements as described in ref. ¹⁹. We illuminated the sample with a circularly polarized laser that has a power of 50 μW and measured the co-polarized PL from the delocalized positively charged trions (2D X⁺) while sweeping an external magnetic field. The results are shown in Fig. 2a, b. The presence of an extra non-radiative channel reduces

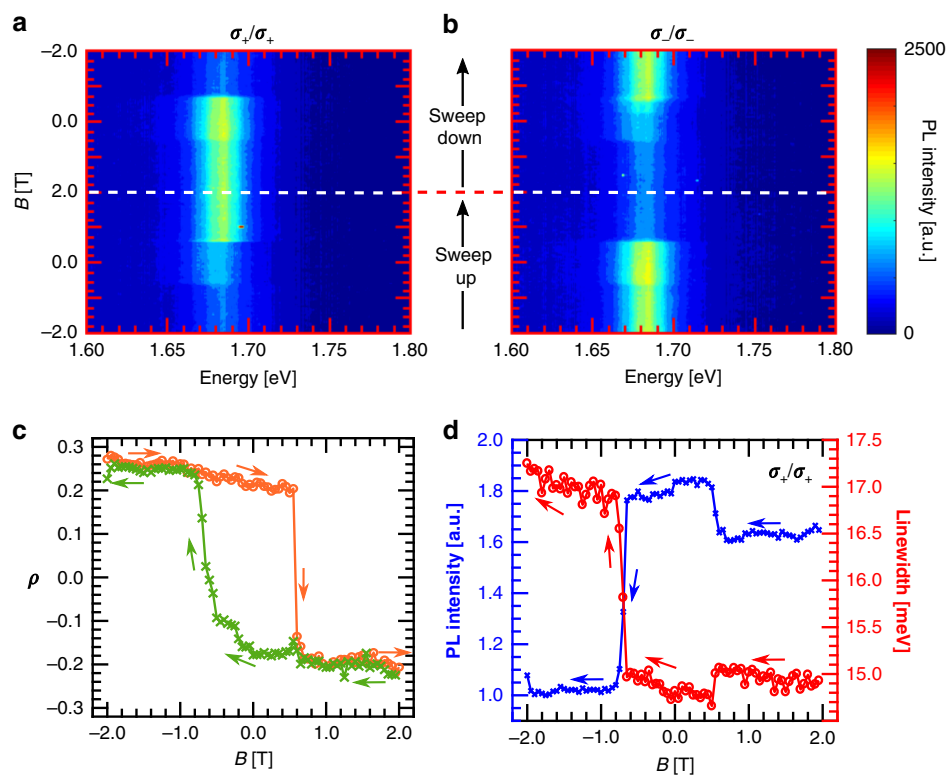


Fig. 2 Charge transfer in CrI_3WSe_2 heterostructure. **a, b** Magneto-PL intensity of the 2D X^+ for right (σ_-) and left (σ_+) circular excitation and collection. The charge transfer is valley selective causing the K and K' valleys to have unequal PL intensity, depending on the spin CrI_3 interfacial layer. The magnetic field is swepted in a loop between ± 2 T. The white dashed line represents the field at which the field sweep direction is inverted. **c** The interfacial CrI_3 layer switches spin hysteretically, which is reflected in the PL polarization ρ . The orange (green) curves show ρ for downward (upward) magnetic field sweeps. **d** The linewidth (red) and intensity (blue) of X^+ of the K valley changes with applied field. There is a correlated increase of linewidth and decrease of intensity.

the PL intensity from that valley of WSe_2 , which aligns with the spin of CrI_3 . It has been shown in ref. ¹⁹ that this effect is governed by spin-dependent charge transfer between the interfacial (top) layer of the CrI_3 and WSe_2 . For quantitative analysis, we measure the PL polarization ρ using

$$\rho(B) = \frac{I_{\sigma_-/\sigma_-} - I_{\sigma_+/\sigma_+}}{I_{\sigma_-/\sigma_-} + I_{\sigma_+/\sigma_+}}, \quad (1)$$

which is shown in Fig. 2c. Here I_{σ_+/σ_+} (I_{σ_-/σ_-}) corresponds to PL intensity for σ_+ (σ_-) excitation and collection. When the spin of top CrI_3 is in the $-z$ ($+z$) direction, the PL from the K' (K) valley is brighter. This leads to a positive (negative) ρ at high magnetic fields in the $-z$ ($+z$) direction. The top layer CrI_3 undergoes a spin-flip transition at ± 0.6 T, which is evident from the sudden jump in ρ at those fields. This also matches well with a typical magnetic field-dependent magnetic circular dichroism trace of bilayer CrI_3 (shown in Supplementary Fig. 2), which also responds to the spin-flip transitions of the CrI_3 layers. Finally, due to the increased non-radiative decay rate, the linewidth of the 2D X^+ of one valley should increase in correlation with a decrease in intensity. We demonstrate this in Fig. 2d with PL from the K valley during the downward magnet sweep. We see that at fields where the linewidth drops, the PL intensity increases and vice versa. This unambiguously proves the existence charge transfer between the two materials.

Observation of site-controlled localized X^+ . Having shown the existence of charge transfer, we now exploit it to increase

the propensity of observing hole-charged single excitons at strained locations near the nanopillars. We measured the PL spectrum at low excitation laser power (500 nW) of linear polarization at 5 nanopillars and found 15 sharp emission lines without resolvable FSS at zero magnetic field. These nanopillars are identified in an optical micrograph in Supplementary Fig. 1. PL spectra at the corresponding locations are presented in Supplementary Fig. 3. To confirm that these emissions arise from hole-charged excitons, we performed polarization unresolved PL measurements under linear excitation. An exemplary magnetic field-dependent PL spectra is shown Fig. 3a. The characteristic “X” shaped dispersion is observed¹⁷. Spectral linecuts at select fields are shown in Fig. 3b. The FSS (Δ) is a linear function of applied field: $\Delta = g_F \mu_B B$, where g_F is the Lande’ g -factor of 0D X^+ and μ_B is the Bohr magneton. For the 0D X^+ emitter shown here, we found a $g_F = 7.4 \pm 0.2$, consistent with previous reports¹⁸. On the contrary, the FSS of localized 0D X^0 shows a starkly different behavior, with a finite zero-field splitting and a quadratic increase at low fields (Supplementary Fig. 4). Furthermore, to rule out the possibility of charged biexcitons we performed power-dependent intensity measurements to investigate the linear response of the PL magnitude to the pump power. Supplementary Figure 5 presents the PL integrated intensity of 0D X^+ , as a function of the excitation power. We observe the power-dependent PL magnitude increases monotonically as P^α , where α is a fit parameter. From the fit, the value of α is 1.02 ± 0.2 . Given that charged biexcitonic intensity increase is more quadratic²⁶, we can rule out its presence.

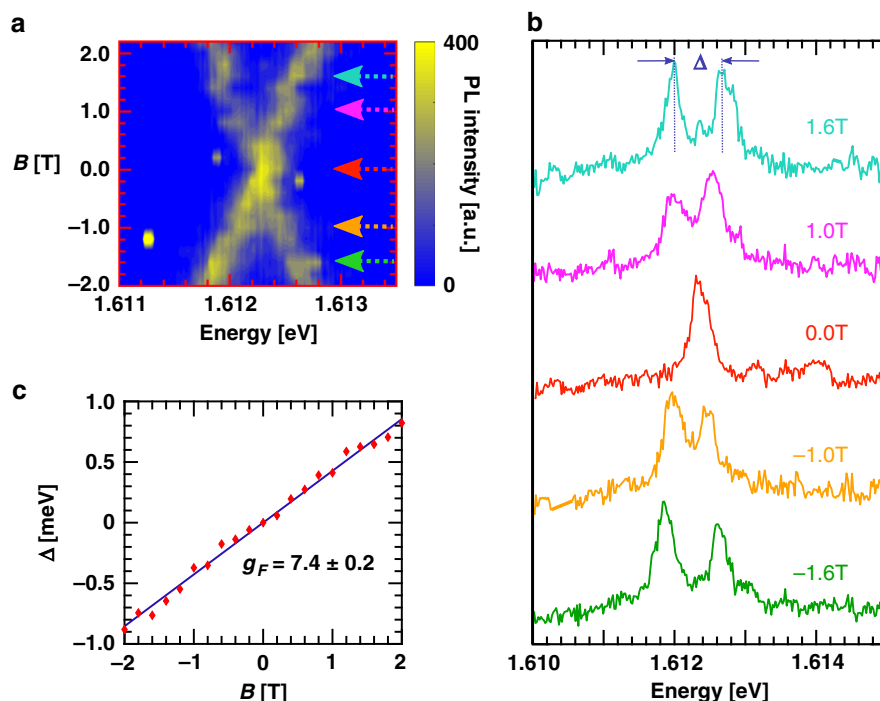


Fig. 3 Magneto-PL of OD X⁺ for linear excitation. The detection does not project into specific polarization states. **a** Colored contour plot of magnetic field-dependent spectrum of OD X⁺. **b** Spectral linecuts for select fields, marked in **a**, are shown. **c** Splitting between the two peaks shows a linear increase with field without any measurable zero-field splitting.

Polarization-resolved magneto-PL of OD X⁺. The fine structure arises from opposite valley-polarized X⁺ modes whose degeneracy is lifted with magnetic field. To confirm this, we performed polarization-resolved magneto-optical measurements for a linearly (circularly) polarized excitation (collection) as a function of applied magnetic fields. Figure 4a, b shows an exemplary polarization-resolved spectral map of OD X⁺. We find that while the σ_+ shifts downward (upward) in energy at positive (negative) magnetic field, the σ_- shows the opposite behavior by showing shifts to higher (lower) energy at positive (negative) magnetic field. The sudden energy jump observed at -1.5 T is due to spectral jittering, common in these kind of devices¹⁷. Figure 4c shows the corresponding polarization-resolved spectral linecuts of the OD X⁺ at select magnetic fields, recorded with spectral resolution of 20 μ eV. At zero field the spectrum clearly shows a single peak with unresolvable FSS. With increasing applied magnetic field, the single peak converts into a doublet and the two components split further apart. We analyzed the degree of circular polarization (DoCP) of each of the modes to study the valley polarization of OD X⁺. The extracted DoCP values of both higher energy and lower energy peaks are plotted in Fig. 4d at different magnetic fields. The DoCP of the σ_+ and σ_- are extracted using

$$\text{DoCP} = \frac{I_{H/\sigma_-} - I_{H/\sigma_+}}{I_{H/\sigma_-} + I_{H/\sigma_+}}, \quad (2)$$

where $I_{H/\sigma_{\pm}}$ is the intensity of the σ_+ (σ_-) polarized emissions for linearly polarized excitation. The DoCP values were extracted for the lower and higher energy peaks by integrating the intensity centered at each peak (depicted by purple and black dashed arrows in Fig. 4c) for both the polarized collection spectrum and use the abovementioned equation. We find that with increasing B fields, the valley degeneracy is lifted due to Zeeman splitting, and the OD X⁺ emission becomes increasingly circularly polarized.

The energy ordering between the two circularly polarized modes inverts with the field direction.

PL polarization (ρ) of OD X⁺. Finally to investigate the role of the proximal CrI₃ layer magnetization, akin to the 2D X⁺, we extract the PL polarization (ρ) for the OD X⁺. This is demonstrated in Fig. 5. In contrast to the DoCP measurements where linearly polarized excitation was used, here we recorded PL with co-polarized *circular* excitation and collection as a function of increasing and decreasing magnetic field sweeps. The magneto-optical spectra are shown in Fig. 5a, b. Spectral linecuts at some select fields are shown in Fig. 5c, d. The extracted ρ has been shown in Fig. 5e. At zero field, we observe a PL polarization difference of close to 15% between the upward and downward sweeps along with a hysteretic feature the region between ± 0.6 T similar to the 2D X⁺ case. The finite intensity contrast in the σ_+ and σ_- modes at zero field is a result of spin-polarized charge transfer from the CrI₃ which prefers positive trion of one polarization over its time reversal pair. This effect is less pronounced for the OD X⁺ than the 2D 0 X⁺. A plausible explanation can be the uncontrolled contact between the CrI₃ and WSe₂ near the pillar tips which can lead to a larger separation between the two layers compared to flat regions in between and away from the pillars.

Discussion

In this work, we have demonstrated the optical excitation of site-controlled OD X⁺ in WSe₂ using band-structure engineering. The type-II band alignment between WSe₂ and CrI₃ promotes p-doping of WSe₂ via charge transfer. We first proved the existence of charge transfer using the PL from delocalized positive trions. At locations of strain-inducing nanopillars, we detected localized emission devoid of FSS at zero applied magnetic field. Quenched electron-hole exchange interactions in OD X⁺ are responsible for

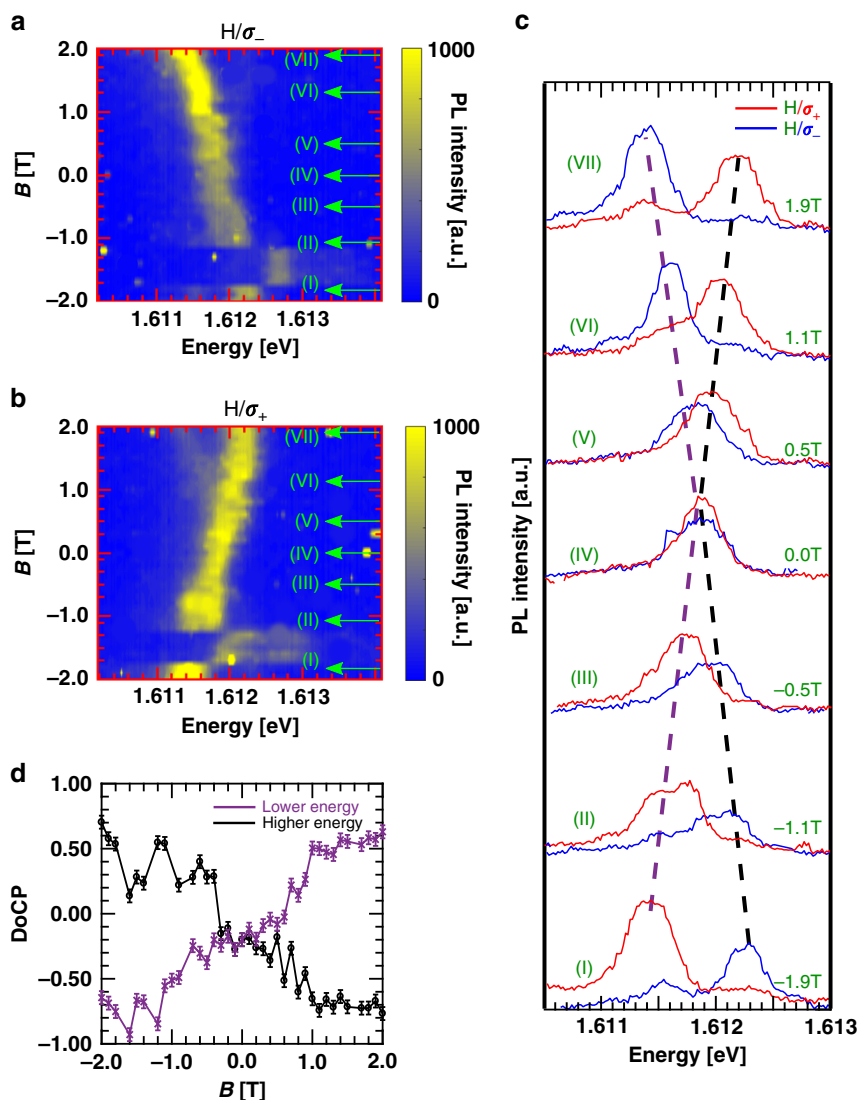


Fig. 4 Polarization-resolved magneto-PL for OD X⁺. Polarization-resolved magneto-PL for linear excitation and **a** σ_- and **b** σ_+ collection. A linear change in energy of the fine-structure levels confirms positively charged excitonic nature of the localized emission. The purple and black dashed lines follow the lower and higher energy modes respectively. **c** Spectral linecuts at select applied fields as indicated in **a**, **b**. **d** The DoCP of the lower (purple) and higher (black) energy modes extracted from **a** and **b**. The circular polarization purity increases with the separation between the modes.

such emission spectrum. We confirmed their presence using polarization-resolved and unresolved magneto-PL experiments. We also demonstrated spin selectivity in the OD X⁺ at zero applied fields, which is a consequence of spin-polarized charge transfer between CrI₃ and WSe₂. We envision that our work will fuel further experimental exploration on engineering nanopatterned substrates which maintain the site-control we demonstrated while enhancing the interaction between OD X⁺ and CrI₃. A strong magnetically coupled OD X⁺ can also serve as an optical probe for nano-scale deformation induced change in magnetic order in CrI₃^{27,28}.

Methods

Sample fabrication. We fabricated gold nanopillars using e-beam lithography and physical vapor deposition on a p-type Si substrate with 300 nm SiO₂ passivation. The pillars were 120 nm in height and had a circular cross section of diameter 300 nm. The HS assembly was done using a layer-by-layer dry transfer technique. Atomically thin flakes were first exfoliated from bulk crystals (from HQ Graphene) onto Si substrates with a 300-nm oxide layer. Flakes of monolayer WSe₂ and bilayer

CrI₃ were identified by their optical contrast. Two thin hBN flakes were chosen to encapsulate the WSe₂/CrI₃ HS. Their thickness was less than 3 nm to ensure good contact of the HS to the substrate with nanopillars. The identified flakes were picked up one-by-one in the order of hBN, WSe₂, CrI₃, and hBN using a stamp that consists of a polycarbonate thin film attached to a polydimethylsiloxane film on a glass slide. The complete stack was pressed and transferred onto the prepatterned nanopillar substrate by melting the polycarbonate thin film at 180 °C. The polycarbonate residue on the device was removed with chloroform and isopropyl alcohol before measurements. The fabrication process involving CrI₃ was performed inside a nitrogen-filled glovebox to avoid oxygen and moisture induced degradation.

PL measurements. All optical measurements are performed using a home-built confocal microscope. The sample is excited using a 633 nm laser focused onto a diffraction spot size 500 nm using a 0.82 NA objective lens in a closed-cycle cryostat (AttoDry 1000) at 4K equipped with a super-conducting magnet. The PL emitted is collected by the same objective and coupled into a single mode fiber. Polarization selection is carried out using linear polarizers and achromatic quarter wave plates (Thorlabs AQWP10M-580) in appropriate order and relative orientations. The light from the collection fiber is analyzed using a Princeton Instruments spectrometer (Acton SP-2750i) with a resolution limit of 20 μ eV.

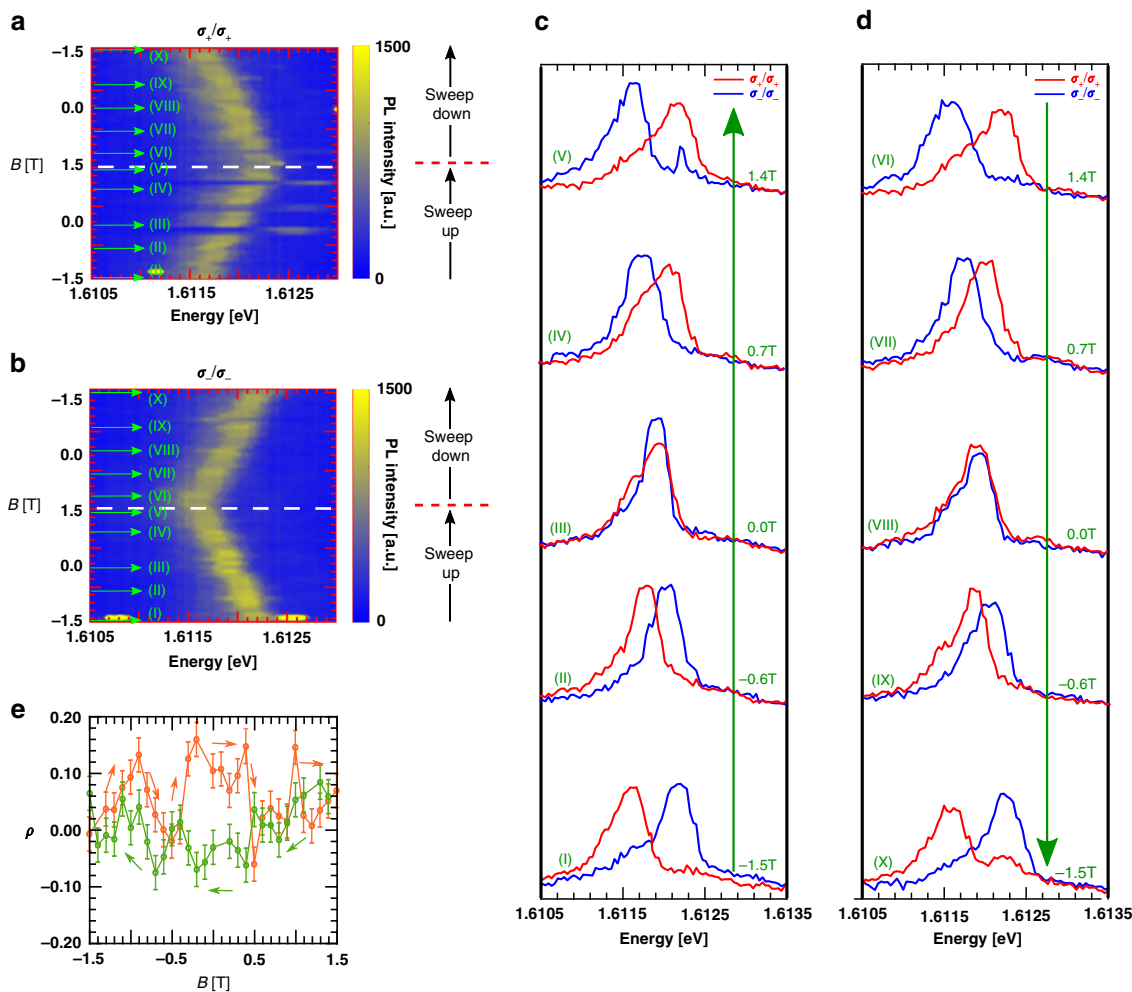


Fig. 5 Co-circular polarized magneto-PL of OD X⁺ spectra for a σ_+ and b σ_- collection and excitation. The applied magnetic field is swept in a loop between ± 1.5 T. The white dashed lines represent the field at which the sweep direction is inverted. **c, d** Spectral linecuts at select applied fields as indicated in **a** and **b**. **e** The PL polarization ρ of OD X⁺ extracted from **a** and **b** using Eq. (2). The orange and green curves represent ρ for upward and downward field sweeps.

Data availability

The datasets generated during and/or analyzed during the current study are available from the corresponding author on reasonable request.

Received: 16 June 2020; Accepted: 30 September 2020;

Published online: 30 October 2020

References

1. Ash, E. A., Pitt, C. W. & Wilson, M. G. F. Integrated optical circuits for telecommunications. *Nature* **261**, 377–381 (1976).
2. Atatüre, M., Englund, D., Vamivakas, N., Lee, S.-Y. & Wrachtrup, J. Material platforms for spin-based photonic quantum technologies. *Nat. Rev. Mater.* **3**, 38–51 (2018).
3. Xiao, D., Liu, G.-B., Feng, W., Xu, X. & Yao, W. Coupled spin and valley physics in monolayers of MoS₂ and other group-VI dichalcogenides. *Phys. Rev. Lett.* **108**, 196802 (2012).
4. Xu, X., Yao, W., Xiao, D. & Heinz, T. F. Spin and pseudospins in layered transition metal dichalcogenides. *Nat. Phys.* **10**, 343–350 (2014).
5. Mak, K. F., He, K., Shan, J. & Heinz, T. F. Control of valley polarization in monolayer MoS₂ by optical helicity. *Nat. Nanotechnol.* **7**, 494–498 (2012).
6. Mak, K. F., McGill, K. L., Park, J. & McEuen, P. L. The valley hall effect in MoS₂ transistors. *Science* **344**, 1489–1492 (2014).
7. Cao, T. et al. Valley-selective circular dichroism of monolayer molybdenum disulphide. *Nat. Commun.* **3**, 887 (2012).

8. Yao, W., Xiao, D. & Niu, Q. Valley-dependent optoelectronics from inversion symmetry breaking. *Phys. Rev. B* **77**, 207–211 (2008).
9. Chernikov, A. et al. Exciton binding energy and nonhydrogenic rydberg series in monolayer WS₂. *Phys. Rev. Lett.* **113**, 076802 (2014).
10. Mak, K. F., Lee, C., Hone, J., Shan, J. & Heinz, T. F. Atomically thin MoS₂: a new direct-gap semiconductor. *Phys. Rev. Lett.* **105**, 136805 (2010).
11. Mak, K. F. et al. Tightly bound trions in monolayer MoS₂. *Nat. Mater.* **12**, 207–211 (2014).
12. Srivastava, A. et al. Optically active quantum dots in monolayer WSe₂. *Nat. Nanotechnol.* **10**, 491–496 (2015).
13. He, Y.-M. et al. Single quantum emitters in monolayer semiconductors. *Nat. Nanotechnol.* **10**, 497–502 (2015).
14. Chakraborty, C., Kinnischtzke, L., Goodfellow, K. M., Beams, R. & Vamivakas, A. N. Voltage-controlled quantum light from an atomically thin semiconductor. *Nat. Nanotechnol.* **10**, 507–511 (2015).
15. Koperski, M. et al. Single photon emitters in exfoliated WSe₂ structures. *Nat. Nanotechnol.* **10**, 503–506 (2015).
16. Chakraborty, C. et al. 3d localized trions in monolayer WSe₂ in a charge tunable van der waals heterostructure. *Nano Lett.* **18**, 2859–2863 (2018).
17. Lu, X. et al. Optical initialization of a single spin-valley in charged WSe₂ quantum dots. *Nat. Nanotechnol.* **14**, 426–431 (2019).
18. Brotons-Gisbert, M. et al. Coulomb blockade in an atomically thin quantum dot coupled to a tunable fermi reservoir. *Nat. Nanotechnol.* **14**, 442–446 (2019).
19. Zhong, D. et al. Van der waals engineering of ferromagnetic semiconductor heterostructures for spin and valleytronics. *Science Advances* **3**, e1603113 (2017).

20. Branny, A., Kumar, S., Proux, R. & Gerardot, B. D. Deterministic strain-induced arrays of quantum emitters in a two-dimensional semiconductor. *Nat. Commun.* **8**, 15053 (2017).
21. Palacios-Berraquero, C. et al. Large-scale quantum-emitter arrays in atomically thin semiconductors. *Nat. Commun.* **8**, 15093 (2017).
22. Zhong, D. et al. Layer-resolved magnetic proximity effect in van der Waals heterostructures. *Nat. Nanotechnol.* **15**, 187–191 (2020).
23. Wang, H., Eyert, V. & Schwingenschlögl, U. Electronic structure and magnetic ordering of thesemiconducting chromium trihalides CrCl₃, CrBr₃, and CrI₃. *J. Phys. Condensed Matter* **23**, 116003 (2011).
24. Zhang, W.-B., Qu, Q., Zhu, P. & Lam, C.-H. Robust intrinsic ferromagnetism and half semiconductivity in stable two-dimensional single-layer chromium trihalides. *J. Mater. Chem. C* **3**, 12457–12468 (2015).
25. Shepard, G. D. et al. Nanobubble induced formation of quantum emitters in monolayer semiconductors. *2D Mater.* **4**, 021019 (2017).
26. You, Y. et al. Observation of biexcitons in monolayer WSe₂. *Nat. Phys.* **11**, 477–481 (2015).
27. Li, T. et al. Pressure-controlled interlayer magnetism in atomically thin CrI₃. *Nat. Mater.* **18**, 1303–1308 (2019).
28. Jiang, S., Xie, H., Shan, J. & Mak, K. F. Exchange magnetostriction in two-dimensional antiferromagnets. *Nat. Mater.* <https://doi.org/10.1038/s41563-020-0712-x> (2020).

Acknowledgements

A.N.V. acknowledges the support by the NSF under Grant NSF-CAREER-DMR-1553788 and NSF-MRSEC-DMR-1719875, and the Air Force Office of Scientific Research under Grant FA9550-19-1-0074. J.S. and K.F.M. acknowledge support from the DOE, Office of Science, Basic Energy Sciences under Award DE-SC0019481.

Author contributions

A.M. fabricated nanopillars array, and designed the optical measurements and built the experimental setup. L.L. fabricated the heterostructure. A.M. and K.S. carried out the optical measurements. L.L. performed the magnetic circular dichroism measurements.

A.M., K.S., A.N.V., J.S., and K.F.M. analyzed the data. All authors discussed the results and co-wrote the final manuscript.

Competing interests

The authors declare no competing interests.

Additional information

Supplementary information is available for this paper at <https://doi.org/10.1038/s41467-020-19262-2>.

Correspondence and requests for materials should be addressed to A.N.V.

Peer review information *Nature Communications* thanks the anonymous reviewers for their contribution to the peer review of this work.

Reprints and permission information is available at <http://www.nature.com/reprints>

Publisher's note Springer Nature remains neutral with regard to jurisdictional claims in published maps and institutional affiliations.



Open Access This article is licensed under a Creative Commons Attribution 4.0 International License, which permits use, sharing, adaptation, distribution and reproduction in any medium or format, as long as you give appropriate credit to the original author(s) and the source, provide a link to the Creative Commons license, and indicate if changes were made. The images or other third party material in this article are included in the article's Creative Commons license, unless indicated otherwise in a credit line to the material. If material is not included in the article's Creative Commons license and your intended use is not permitted by statutory regulation or exceeds the permitted use, you will need to obtain permission directly from the copyright holder. To view a copy of this license, visit <http://creativecommons.org/licenses/by/4.0/>.

© The Author(s) 2020